J Mater Sci (2011) 46:2140–2147
DOI 10.1007/s10853-010-5050-y

# Preparation, structure, and electrochemical performance of anodes from artificial graphite scrap for lithium ion batteries

**Chang-ling Fan · Han Chen**

Received: 13 July 2010 / Accepted: 2 November 2010 / Published online: 23 November 2010


**Abstract** Artificial graphite scrap prepared from petroleum coke with low degree of graphitization was further graphitized under various conditions. Different categories of coke were also treated with the optimum technology. The prepared samples were characterized with X-ray diffraction, ash content determination, morphology observation, and galvanostatic charge and discharge. It was shown in the experiments that the heat treatment temperature should be increased to 2800 °C to remove impurities. Slow heating rate and evacuation technology were beneficial to the growth of graphite crystallite and the improvement of discharge capacity. And the latter condition possessed the larger influences, especially on the growth of crystallite dimension in the b axis direction, degree of graphitization, and discharge capacity. The sample D-3000 prepared from pure needle coke possessed the maximum discharge capacity of 342.1 $mAhg^{-1}$ among all prepared samples. The linear regression equations between the volume of graphite crystallite and discharge capacity were established.

C. Fan (✉)
College of Materials Science and Engineering,
Hunan University, Changsha, Hunan 410082,
People's Republic of China
e-mail: clfanhd@yahoo.com.cn

H. Chen
School of Metallurgical Engineering, Hunan University
of Technology, Zhuzhou, Hunan 412000,
People's Republic of China

## Introduction

Graphite materials including natural graphite and artificial graphite have been widely studied as anodes for lithium ion batteries due to their attractive characteristics, such as low potential platform, high capacity, and good reversibility [1, 2]. Recently, silicon [3, 4], tin [5, 6], and spinel $Li_4Ti_5O_{12}$ [7] have been considered as the promising candidate anodes. The theoretical capacities of silicon and tin were very high, but the huge volume changes led to mechanical failure in the lithium alloying and dealloying process. $Li_4Ti_5O_{12}$ possessed a very long cyclic life because of zero-strain characteristic, but its potential platform was higher (1.55 V, vs. $Li^+/Li$) compared to graphite (0.1 V, vs. $Li^+/Li$).

The cyclic performances of natural graphite [8] were poor because graphene layers which were combined with weak van der Waals force were easy to exfoliate. It was often coated with various materials to enhance its cyclic performances [9–11]. Graphitized soft carbons, such as petroleum coke, needle coke, carbon fiber [12–14], and mesocarbon microbead (MCMB) [15] were the representative materials of artificial graphite. Artificial graphite possessed excellent cyclic performances compared to natural graphite due to its stable structure during the intercalation and deintercalation process. Among all the artificial graphite anodes of lithium ion batteries, MCMB possessed spherical morphology and stable structure and was often utilized as industry anode materials [16, 17]. However, the main drawbacks of MCMB were their long production flow and high manufacture cost. And carbon fiber had the similar disadvantages and few were used as anode.

However, irreversible reactions led to the formation of solid electrolyte interphase (SEI) film of artificial graphite anodes during the initial cycle, and its efficiency was low.

Modifications with various methods [18–21] were effective approaches to overcome this disadvantage. No matter what kinds of modifications will be carried out on artificial graphite, the core material (artificial graphite) must possess well-developed structures for storing lithium ions and have satisfactory electrochemical performances. Therefore, the preparation of artificial graphite anodes still played an important role.

The production flow of anode by the directly graphitization of soft carbons (such as petroleum coke and needle coke) was very short compared with MCMB and their production cost was also low. Ma et al. [22] studied the electrochemical characteristics of petroleum coke, pitch coke, needle coke, metallurgical coke, and MCMB prepared at different temperatures. Tran et al. [23] studied the effects of heat treatment temperature (HTT) on petroleum cokes for anode. Lu et al. [24] investigated the influences of the microstructures and surface compositions on the irreversible capacity of pitch-based carbon. Alcántara et al. [25] studied the effects of mechanical grinding on the electrochemical and microstructure of graphitized petroleum coke. Lia et al. [26] investigated the influences of fluorination on the electrochemical characteristics and surface structure of graphitized petroleum cokes. Kang et al. [27] studied the electrochemical characteristics of carbonized needle coke. However, systematic investigations on the graphitization conditions and related technologies were few for technological confidentiality or limit of graphitization equipment. Previous researches mainly focused on the further modifications of artificial anode products from supplier, not the preparation of artificial graphite.

In this article, the preparation conditions and technologies of further graphitization of artificial graphite scrap were investigated. Furthermore, graphite products based on different cokes were studied, and the relationships between the volume of graphite crystallite and discharge capacity were also investigated.

## Experimental

### Sample preparation

All the samples of artificial graphite scraps were further graphitized in a middle frequency induction furnace. The atmosphere in the furnace was vacuumed to a pressure of 1.3 Pa before heating. Evacuation technology was applied during graphitization until the HTT reaches 2400 °C. Then vacuum pump was turned off and high purity argon gas was introduced into the furnace to a pressure of 0.1 MPa. Next, samples were graphitized to various HTTs. Samples thus obtained were ground to pass the 325 mesh standard sieve. In order to investigate the influences of evacuation technology, sample was also graphitized in argon gas at the pressure of 0.1 MPa. Two heating rates (10 and 30 °C $min^{-1}$) were applied, respectively.

### Material characterization

The crystalline structures of samples were characterized by an X-ray diffractometer (XRD) with Cu $K_\alpha$ radiation over an angular $2\theta$ range from 15 to 80° (D5000, Siemens Company, Germany). The ash content was determined by burning artificial graphite at 750 °C in air for 3 h in a muffle furnace. The particle morphologies of the powder samples were observed by a Hi-scope advanced microscope (KH-3000VD, Hirox Company, Japan).

### Electrochemical characterization

The galvanostatic experiments were performed by a battery testing instrument (BT2000, Arbin Company, USA). The working electrode consisted of a mixture of 89 wt% artificial graphite, 6 wt% acetylene black, and 5 wt% polytetrafluorethylene (PTFE) binder. The counter and reference electrodes were lithium foil. The electrolyte was made by 1 mol $L^{-1}$ $LiClO_4$ dissolved in the solvent mixture of ethylene carbonate and diethyl carbonate in the mass ratio of 1:1. The batteries were charged and discharged between 0.000 and 2.000 V (vs. $Li^+/Li$) at the current density of 15.000 $mAg^{-1}$.

## Results and discussion

### Necessity of further graphitization

An artificial graphite electrode scrap (sample A) with the aggregate of petroleum coke was used to study the conditions of further graphitization. The XRD spectrum and its corresponding structural parameters are shown in Fig. 1 and Table 1.

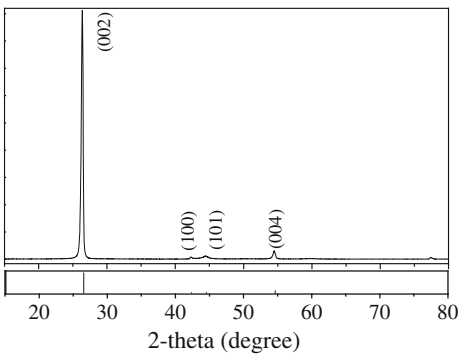


**Fig. 1** XRD spectrum of sample A

**Table 1** Structural parameters of sample A

| Sample | $d_{002}$ (nm) | $L_{002}$ (nm) | $L_{100}$ (nm) | $L_{101}$ (nm) | $G$ (%) |
|---|---|---|---|---|---|
| A | 0.33671 | 28.1 | 26.1 | 5.3 | 84.8 |

It can be seen in Fig. 1 that the peak position and relative intensity of peaks (002), (100), (101), and (004) of sample A are close to the standard spectra of graphite in the bottom (standard card 41-1487). It indicates that it possesses a typical graphite crystalline structure. In addition, a narrow and sharp peak (002) also means that the crystallization is integrity and the defects are comparatively few.

Table 1 shows that the degree of graphitization ($G$) of sample A is 84.8% which is much lower than 100%. The crystallite dimension in the direction of c axis ($L_{002}$), a axis ($L_{100}$), and b axis ($L_{101}$) are 28.1, 26.1, and 5.3 nm, respectively. It indicates that the size of graphite crystallite is small and the HTT of graphitization applied is not very high because the high degree of graphitization lowers the mechanical properties of graphite electrode.

The galvanostatic charge and discharge curves in the first three cycles are presented in Fig. 2.

The SEI forms at about 0.75 V (vs. $Li^+/Li$) in the initial charge process. It disappears in the next cycle which shows that the formation of SEI film is complete in the first cycle. Therefore, the discharge capacity in the third cycle can be adopted as standard to evaluate the electrochemical performance of graphite anode. Discharge capacities in the following texts are all referred to the capacity in the third cycle. The discharge capacity of sample A in the third cycle is 291.9 $mAhg^{-1}$ which is much lower than the theoretical capacity of 372 $mAhg^{-1}$. The low capacity is in accordance with the low degree of graphitization and small size of graphite crystallite of sample A. In order to be applied as anode for advanced lithium ion batteries, the artificial graphite is quite necessary to be further graphitized.

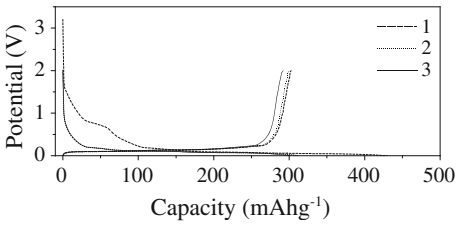


**Fig. 2** Charge and discharge curves of sample A in the first three cycles

## Influences of HTT

Sample A was further graphitized to various HTTs at the slow heating rate. And the evacuation technology was also employed. Sample A-2500 represented that the sample A was graphitized at the HTT of 2500 °C. The structural parameters and discharge capacities in the third cycle of samples A are shown in Table 2.

One can see that the discharge capacities of sample A remain almost unchanged even if $L_{002}$, $L_{100}$, and $L_{101}$ of graphite crystallite gradually increases at HTT are lower than 2800 °C. However, the discharge capacity of sample A increases suddenly to 330.2 $mAhg^{-1}$ when HTT reaches 2800 °C. The discharge capacity of sample A-3000 increases only 6.8 $mAhg^{-1}$ compared to sample A-2800 while HTT increases from 2800 to 3000 °C. As a result, 2800 °C is selected as the optimum HTT for saving energy and lowering cost.

## Content and composition of impurities

In order to find the reasons that block the increasing of discharge capacity when HTT is lower than 2800 °C, the ash content and its compositions were determined. The ash content of samples A, A-2500, and A-2800 are given in Table 3.

**Table 3** Ash content of samples A, A-2500, and A-2800

| Samples | A | A-2500 | A-2800 |
|---|---|---|---|
| Ash content (%) | 0.27 | 0.16 | 0.03 |

**Table 2** Structural parameters and discharge capacities in the third cycle of samples A graphitized with various HTTs

| Samples | $d_{002}$ (nm) | $L_{002}$ (nm) | $L_{100}$ (nm) | $L_{101}$ (nm) | $G$ (%) | Capacity ($mAhg^{-1}$) |
|---|---|---|---|---|---|---|
| A | 0.33671 | 28.1 | 26.1 | 5.3 | 84.8 | 291.9 |
| A-2500 | 0.33666 | 28.7 | 26.8 | 6.6 | 85.4 | 291.7 |
| A-2600 | 0.33658 | 29.7 | 28.2 | 7.1 | 86.3 | 293.6 |
| A-2700 | 0.33637 | 30.2 | 30.1 | 7.8 | 88.7 | 300.7 |
| A-2800 | 0.33628 | 31.0 | 31.8 | 8.5 | 89.8 | 330.2 |
| A-2900 | 0.33626 | 31.6 | 32.4 | 8.9 | 90.0 | 330.8 |
| A-3000 | 0.33614 | 32.2 | 33.5 | 9.4 | 91.4 | 337.0 |

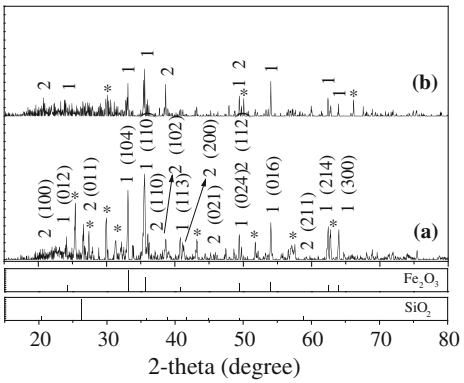


**Fig. 3** XRD spectra of the ash of samples A (*a*) and A-2500 (*b*), the two standard spectra shown below are $Fe_2O_3$ (*top*) and $SiO_2$ (*bottom*)

It can be seen from Table 3 that the ash content of samples A and A-2500 are 0.27 and 0.16%, respectively. The content of ash in sample A drops at a ratio of 41% when HTT increases to 2500 °C. From Table 2, we also find that the discharge capacities of sample A increase very slowly with the increasing of HTT when the HTT is lower than 2800 °C. Very low ash content (0.03%) of sample A-2800 indicates that impurities are eliminated when HTT reaches 2800 °C. Therefore, the discharge capacity of sample A increases suddenly to 330.2 $mAhg^{-1}$. It can be concluded that discharge capacity of sample A reaches a rather high value of 330.2 $mAhg^{-1}$ when impurities are eliminated thoroughly at 2800 °C.

Figure 3 gives the XRD spectra of ash of samples A and A-2500. The standard spectrum of $Fe_2O_3$ (top) and $SiO_2$ (bottom) is also given in the figure. We find that the main peaks of ash are in accordance with those of $Fe_2O_3$ and $SiO_2$. The corresponding peak index is labeled above the peaks. And the number of 1 or 2 before the peak index which represents $Fe_2O_3$ or $SiO_2$ is also added. There are also some other peaks we cannot identify and labeled with asterisk. By comparing with the standard spectrum of $Fe_2O_3$ and $SiO_2$, we know that the position and relative intensity of main peaks in Fig. 3a are nearly equivalent. Only the two peaks which possess the largest and the second largest intensities are not in the right order. This phenomenon also emerges in some other researches. For example, the order of the peaks (200) and (131) of $LiFePO_4$ in synthesized sample is often contradicted with the standard spectra [28]. The intensities of the main peaks of $Fe_2O_3$ decreases to half of those of sample A while HTT increases to 2500 °C (sample A-2500). And peaks of $SiO_2$ nearly disappear while HTT reaches 2500 °C. It is in accordance with the analysis of the ash content.

However, it does not mean that impurities in sample A are $Fe_2O_3$ and $SiO_2$, but make up of element silicon and iron in that the ash is the burning resultant of artificial graphite under atmosphere.

It is well known that artificial graphite electrode in carbon materials plant is graphitized in Acheson furnace. The furnace bed is built by the concrete and clay brick which are fire-resistant and they can be used safely under 1300 °C. In order to protect the furnace bed, a layer of quartz sand ($SiO_2$) with certain thickness is spread and tamped on it. Then, layers made up of quartz sand and metallurgical coke is also spread. During the graphitization process, quartz sand and metallurgical coke react in high temperature and silicon gas is formed:

$$SiO_2 + C \rightarrow SiO + CO$$

$$SiO + C \rightarrow Si + CO.$$

Silicon gas goes up and penetrates the graphite products. Then it reacts with carbon element in graphite electrode and SiC is formed. Therefore, impurities made by element silicon should be SiC.

In the production of graphite electrode, iron oxide has the catalytic effect on the degree of graphitization of various forms carbon materials such as needle coke, binder pitch, and coal tar pitch [29]. Iron oxide is also used to inhibit the puffing which is caused by element sulfur in petroleum coke. Therefore, $Fe_2O_3$ is often added in the aggregate to improve the performances of graphite electrode. Excess $Fe_2O_3$ will remain in the graphitization electrode. It can be concluded that the impurities made by element iron should be $Fe_2O_3$.

Based on the above comprehensive analysis, we conclude that the impurities of sample A are SiC and $Fe_2O_3$, and they can be eliminated by increasing HTT to 2800 °C.

## Influences of heating rates

In order to investigate the influence of heating rates on the structure and electrochemical performance of sample A, two heating rates were employed. The quick one was 30 °C $min^{-1}$ and the other was 10 °C $min^{-1}$. Sample A was graphitized at the HTT of 2800 °C with the two heating rates, respectively, and the evacuation technology was applied. The prepared samples were labeled as

**Table 4** Structural parameters and discharge capacities in the third cycle of samples A graphitized at 2800 °C with various heating rates

| Samples | $d_{002}$ (nm) | $L_{002}$ (nm) | $L_{100}$ (nm) | $L_{101}$ (nm) | $G$ (%) | Capacity ($mAhg^{-1}$) |
|---|---|---|---|---|---|---|
| A-2800-30C | 0.33629 | 28.8 | 27.4 | 8.4 | 89.7 | 316.4 |
| A-2800-10C | 0.33628 | 31.0 | 31.8 | 8.5 | 89.8 | 330.2 |

A-2800-30C and A-2800-10C, respectively. Their structural parameters and discharge capacities are presented in Table 4.

One can see that the $L_{002}$ and $L_{100}$ of sample A-2800-10C are 2.2 and 4.4 nm larger than those of sample A-2800-30C, respectively. It shows that the slow heating rate help to prompt the growth of graphite crystallite in the direction of (002) and (100). However, the influence of slow heating rate on the growth of crystallite in the direction of (101) is only 0.1 nm which is very little. And the degree of graphitization increases only 0.1%. Therefore, the storage spaces for lithium ions increases and results in an increasing of discharge capacity. The discharge capacity of sample A-2800-10C is 330.2 $mAhg^{-1}$ which is 13.8 $mAhg^{-1}$ larger than that of sample A-2800-30C. It can be concluded that slow heating rate is favorable to the preparation of high capacity anode.

## Influences of evacuation technologies

Two technologies were applied to study the effect of evacuation. One was graphitized sample A in vacuum before 2400 °C and the other was graphitized sample in argon gas at a pressure of 0.1 MPa. The optimum HTT and heating rate were employed, i.e., 2800 °C and 10 °C $min^{-1}$, respectively. The corresponding samples were labeled as A-2800-V and A-2800-Ar, respectively. The experimental results are shown in Table 5.

It shows that the $L_{002}$ and $L_{100}$ of sample A-2800-V are 3.3 and 3.1 nm bigger than those of sample A-2800-Ar, which is similar to the influence of slow heating rate. And the $L_{101}$ of sample A-2800-V which is prepared with the evacuation technology increases 0.7 nm compared to the sample graphitized in an atmosphere of argon gas. The degree of graphitization of sample A-2800-V is also larger (0.7%) than that of sample A-2800-Ar. It means that the influences of evacuation technology are evidently larger than that of heating rate, especially on $L_{101}$ and the degree of graphitization. Therefore, sample A-2800-V possesses the higher discharge capacity of 330.2 $mAhg^{-1}$ which is 11% larger than that of sample A-2800-Ar. This may be due to the evacuation technology which is beneficial to the removing of impurities in artificial graphite which prevent graphite crystallite from growing.

## Influences of the categories of coke

In order to investigate the influences of categories of coke, samples B, C, and D which were made from petroleum coke and needle coke were employed. Sample B was obtained from high purity graphite scrap based on petroleum coke. Sample C was received from high power graphite electrode whose aggregate is needle coke. Sample D was pure needle coke. It should be noted that all the samples were collected from inside of the products with care to minimize the effect of impurities. Samples B, C, and D were further graphitized at various HTTs with the optimum conditions of slow heating rate and the evacuation technology. Figure 4 shows the micrographs of the artificial graphite samples of B, C, and D prepared at the HTT of 3000 °C. The structural parameters and discharge capacities of the above samples are presented in Table 6.

In Fig. 4c, we find that sample D possesses a typical needle morphology. The color of its particle is silver gray and it has obvious metallic luster. In order to observe the particle clearly, all the background of the micrographs was adjusted to gray. Its aspect ratio is high and it is easily graphitized. Partial particles of sample C (Fig. 4b) possess the similar features of needle coke: needle morphology, silver gray, and high aspect ratio. However, the other particles are in black color and their aspect ratio is very low, which is the features of petroleum coke particle. The particle morphology of sample B (Fig. 4a) belongs to petroleum coke. Some particles are black and others are metallic luster. And it possesses low aspect ratio.

It can be seen from Table 6 that the $L_{002}$, $L_{100}$, $L_{101}$, and $G$ of the original samples B, C, and D are smaller than those of samples graphitized at 2400 °C. Therefore, it can be predicted that the HTTs of the three samples are lower than 2400 °C. And the discharge capacities are not very high. Therefore, it is necessary for these samples to be further graphitized with higher HTT.

We can also see that the $L_{002}$, $L_{100}$, $L_{101}$, and $G$ of sample B increase with the increasing of HTT, and the value of $d_{002}$ decreases at the same time. It means that the dimensions of graphite crystallite increase and the numbers of graphene layers become more and more. Therefore, the discharge capacity of sample B increases due to the increasing of the storage space for lithium ions. When HTT

**Table 5** Structural parameters and discharge capacities in the third cycle of samples A graphitized at 2800 °C with various evacuation technologies

| Samples | $d_{002}$ (nm) | $L_{002}$ (nm) | $L_{100}$ (nm) | $L_{101}$ (nm) | $G$ (%) | Capacity ($mAhg^{-1}$) |
|---|---|---|---|---|---|---|
| A-2800-Ar | 0.33634 | 27.7 | 28.7 | 7.8 | 89.1 | 296.1 |
| A-2800-V | 0.33628 | 31.0 | 31.8 | 8.5 | 89.8 | 330.2 |

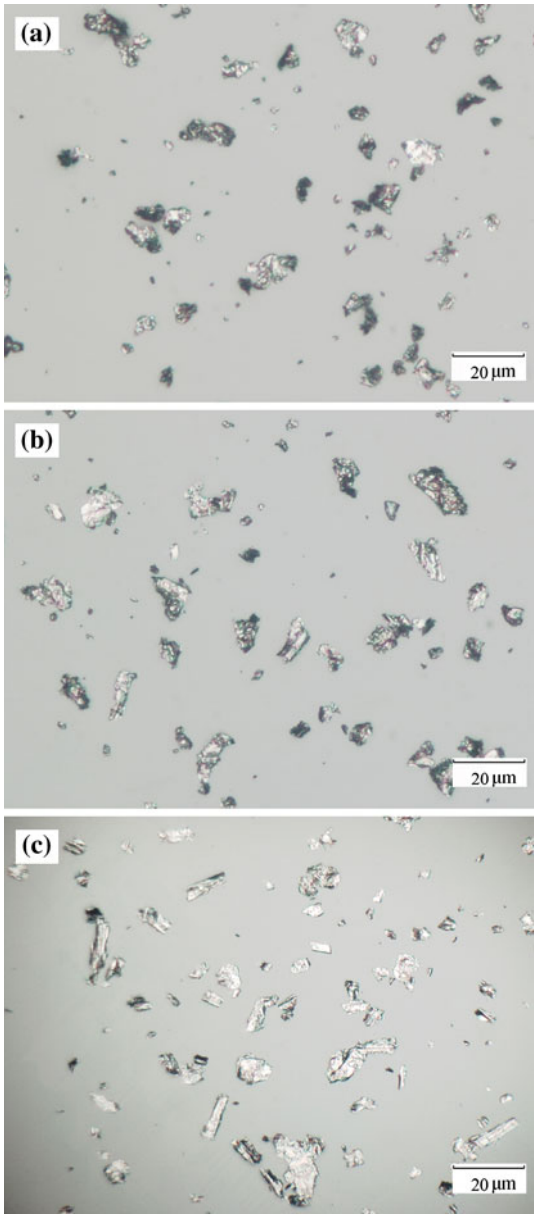


**Fig. 4** Micrographs of samples B **a**, C **b**, and D **c** prepared with the optimum conditions and the HTT of 3000 °C

reaches 3000 °C, the discharge capacity of sample B-3000 is 325.8 $mAhg^{-1}$ which is 22.1 $mAhg^{-1}$ larger than that of the original sample B.

It shows that the crystallite dimensions of samples C and D which are made from needle coke are bigger than sample B. The crystallite dimensions of the original samples C and D are even larger than those of sample B-3000. Therefore, the discharge capacities of samples C and D are larger than those of sample B which is graphitized at the same HTT. This is mainly because needle coke is easier to be graphitized than petroleum coke. Samples C and D are both made from needle coke, but the structure and performance of the former are inferior to the latter due to the side effect of pitch binder in sample C. The discharge capacity of sample D-3000 which is graphitized with the HTT of 3000 °C is 342.1 $mAhg^{-1}$, which approaches to the theoretical capacity of 372 $mAhg^{-1}$. Of all the prepared samples, sample D-3000 possesses the maximum discharge capacity.

## Relationship between the volume of graphite crystallite and discharge capacities

Researches show that lithium ions are intercalated into graphite and lead to the formation of graphite intercalation compounds (GIC). When the stage 1 of GIC is formed ($LiC_6$), every graphene layer is intercalated with one layer of lithium ions; the discharge capacity approaches to the theoretical capacity of 372 $mAhg^{-1}$. At this time, every six carbon atoms in one layer of graphite accommodate one lithium ion [30, 31]. However, references about the influences of graphite crystallite size on the discharge capacity are very few. Iijima et al. [31] and Wissler [32] considered that the discharge capacity of graphite anode is mainly determined by the crystallite size of graphite. Wissler also believed that the larger the crystals are, the higher the specific capacity is. But they did not give more details on the relations.

Can we calculate the accurate capacity magnitude of graphite anode without performing complex galvanostatic charge and discharge experiments? The capacity of graphite anode is related to the graphite crystallite. However, it is almost impossible to determine the discharge capacity exactly because we cannot calculate the numbers of carbon atom in every graphene layer. It is well known that graphite particle is made up of many crystallites and amorphous carbon materials. And, we are unable to know the specific content of graphite crystallite in a particle. It can only be said that the discharge capacity of graphite is related to the volume of graphite crystallite. Here, a method is presented to estimate the discharge capacity of graphite anode through the calculation of the volume of graphite crystallite. The volume of graphite crystallite ($V$) can be calculated from the equation:

$$V = (L_{002}/d_{002} - 1) \times L_{100}^2.$$

In the equation, the value of $L_{002}/d_{002}$ represents the integral numbers of graphene layer in one graphite crystallite.

The volumes of graphite crystallite of samples B, C, and D are calculated. The linearity relations between the volume of graphite crystallite ($V$) and their discharge capacity (DC) are given in Fig. 5. The linearity equations of samples B, C, and D are as follows:

**Table 6** Structural parameters and discharge capacities in the third cycle of samples B, C, and D graphitized with various HTTs under the optimum heating rate and evacuation technology

| Samples | $d_{002}$ (nm) | $L_{002}$ (nm) | $L_{100}$ (nm) | $L_{101}$ (nm) | $G$ (%) | Capacity ($mAhg^{-1}$) |
|---|---|---|---|---|---|---|
| B | 0.33747 | 25.8 | 12.8 | 4.9 | 75.93 | 313.1 |
| B-2400 | 0.33703 | 26.9 | 14.6 | 5.2 | 81.05 | 316.0 |
| B-2600 | 0.33694 | 27.4 | 15.2 | 5.5 | 82.09 | 320.1 |
| B-2800 | 0.33679 | 27.9 | 15.6 | 5.7 | 83.84 | 321.2 |
| B-3000 | 0.33661 | 28.0 | 15.9 | 6.0 | 85.93 | 323.5 |
| C | 0.33685 | 28.1 | 21.7 | 7.1 | 83.14 | 318.4 |
| C-2400 | 0.33659 | 29.5 | 23.2 | 7.6 | 86.16 | 325.8 |
| C-2600 | 0.33648 | 29.6 | 24.1 | 7.6 | 87.44 | 329.7 |
| C-2800 | 0.33634 | 30.1 | 24.6 | 7.8 | 89.07 | 332.9 |
| C-3000 | 0.33612 | 30.4 | 25.1 | 7.9 | 91.63 | 337.5 |
| D | 0.33657 | 37.3 | 23.9 | 8.3 | 86.40 | 322.3 |
| D-2400 | 0.33639 | 41.7 | 25.4 | 8.8 | 88.49 | 326.2 |
| D-2600 | 0.33623 | 44.2 | 28.0 | 9.0 | 90.35 | 336.9 |
| D-2800 | 0.33611 | 45.1 | 29.2 | 9.2 | 91.74 | 340.9 |
| D-3000 | 0.33599 | 46.7 | 31.4 | 9.6 | 93.14 | 342.1 |

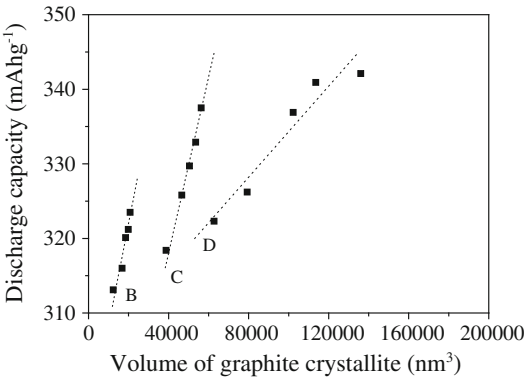


**Fig. 5** Relationship between the volume of graphite crystallite ($V$) and discharge capacities (DC) of samples B, C, and D graphitized with various HTTs under the optimum heating rate and evacuation technology

Sample B: $DC = 297.4 + 0.00121 \times V$, $R = 0.9665$

Sample C: $DC = 276.9 + 0.00106 \times V$, $R = 0.9948$

Sample D: $DC = 304.1 + 0.00030 \times V$, $R = 0.9630$.

It can be seen that the correlation coefficients ($R$) of the linear regression of samples B, C, and D are 0.9665, 0.9948, and 0.9630, respectively. The correlation coefficients are higher than 0.95, which shows that the above hypothesis is reasonable. Therefore, it is reliable to predict the discharge capacity from the volume of graphite crystallite which can be calculated from the XRD analysis.

The discharge capacity of graphite sample can be estimated when the linear regression equation is established. For example, if the structural parameters of sample C based on needle coke is received as following: $L_{002} = 29.7$ nm, $d_{002} = 0.33641$ nm and $L_{100} = 24.3$ nm, then its discharge capacity can be estimated.

The $V$ value of sample C is

$$V = (L_{002}/d_{002} - 1) \times L_{100}^2 = (29.7/0.33641 - 1) \times 24.3^2 = 51372.63\ \text{nm}^3.$$

The discharge capacity DC is

$$DC = 276.9 + 0.00106 \times V = 276.9 + 0.00106 \times 51372.63 = 331.4\ \text{mAhg}^{-1}.$$

However, it should be noted that the linear equations of artificial graphite from different cokes vary due to their differences in carbon resources, granularities, morphology, specific surface area, and so on.

## Conclusion

The HTT of artificial graphite scrap from carbon plants will not be very high because the high degree of graphitization lowers the mechanical properties of graphite electrode. It is necessary to be further graphitized before be used as anode for lithium ion batteries. Impurities in sample A whose aggregate is petroleum coke prevent the discharge capacity from increasing when HTT is lower than 2800 °C. The impurities are composed of SiC and $Fe_2O_3$ and they can be eliminated by enhancing HTT to 2800 °C. The discharge capacity of sample A prepared with the optimum HTT is 330.2 $mAhg^{-1}$. Slow heating rate and evacuation technology are both contributed to the growth of graphite crystallite and the improvement of charge and discharge

performance. The latter condition possesses the larger influences, especially on the growth of $L_{101}$, graphitization degree and discharge capacity. Samples prepared from easily graphitized needle coke have the larger graphite crystallite and higher electrochemical performance compared to petroleum coke. The sample D-3000 prepared from the pure needle coke possesses the maximum discharge capacity of 342.1 $mAhg^{-1}$, which approaches to the theoretical capacity of 372 $mAhg^{-1}$. The discharge capacity of artificial graphite anode is mainly determined by the volume of graphite crystallite and the discharge capacity can be estimated by the linear regression equation based on XRD data.

**Acknowledgements** Authors would like to thank the Bureau of Science and Technology of Hunan Province (No. 00GK1006) and Chinese Ministry of Education (No. 20060532018) for their financial support.

## References

1. Guo HJ, Li XH, Zhang XM, Wang HQ, Wang ZX, Peng WJ (2007) New Carbon Materials 22:7
2. Kwak G, Park J, Lee J, Kim S, Jung I (2007) J Power Sources 174:484
3. Zuo PJ, Yin GP, Ma YL (2007) Electrochim Acta 52:4878
4. Zuo PJ, Wang ZB, Yin GP, Jia DC, Cheng XQ, Du CY, Shi PF (2008) J Mater Sci 43:3149. doi:10.1007/s10853-008-2500-x
5. Qiao H, Zheng Z, Zhang LZ, Xiao LF (2008) J Mater Sci 43:2778. doi:10.1007/s10853-008-2510-8
6. Popova E, Dimitriev Y (2007) J Mater Sci 42:3358. doi:10.1007/s10853-006-0787-z
7. Wang D, Ding H, Song XH, Chen CH (2009) J Mater Sci 44:198. doi:10.1007/s10853-008-3104-1
8. Yoshio M, Wang H, Fukuda K, Hara Y, Adachi Y (2000) J Electrochem Soc 147:1245
9. Zhou YF, Xie S, Chen CH (2005) Electrochim Acta 50:4728
10. Zhang HL, Liu SH, Li F, Bai S, Liu C, Tan J, Cheng HM (2006) Carbon 44:2212
11. Wang J, Chen MM, Wang CY, Hu BQ, Zheng JM (2010) Mater Lett 64:2281
12. Imanishi N, Kashiwagi H, Ichikawa T, Takeda Y, Yamamoto O, Inagaki M (1993) J Electrochem Soc 140:315
13. Tatsumi K, Zaghib K, Sawada Y (1997) J Electrochem Soc 144:2968
14. Kimihito S, Takashi I, Masataka W (1999) Electrochim Acta 44:2185
15. Gabrielle N, Xiang YS, Monique M, Abdelbast G, Gessie B, Kimio K, Karim Z (2002) J Power Sources 108:86
16. Arrebola JC, Caballero A, Hernán L, Morales J (2008) J Power Sources 183:310
17. Kobayashi H, Sakaebe H, Komoto K, Kaneko S, Kageyama H, Tabuchi M, Tatsumi K, Yonemura M, Kanno R, Kamiyama T (2004) Solid State Ion 175:229
18. Yoon SH, Kim HJ, Oh SM (2001) J Power Sources 94:68
19. Zhang YG, Wang CY, Yan P (2007) J Inorg Mater 22:622
20. Chou CS, Tsou CH, Wang CI (2008) Adv Powder Technol 19:383
21. Ohta N, Nagaoka K, Hoshi K, Bitoh S, Inagaki M (2009) J Power Sources 194:985
22. Ma SH, Li J, Jing XB, Wang FS (1996) Solid State Ion 86–88:911
23. Tran TD, Spellman LM, Goldberger WM, Song X, Kinoshita K (1997) J Power Sources 68:106
24. Lu W, Chung D (2003) Carbon 41:945
25. Alcántara R, Lavel P, Ortiz GF, Tirado JL, Menéndez R, Santamaría R, Jiménez JM (2003) Carbon 41:3003
26. Lia J, Naga K, Ohzawa Y, Nakajima T, Shames AI, Panich AM (2005) J Fluor Chem 126:265
27. Kang HG, Park JK, Han BS, Lee H (2006) J Power Sources 153:170
28. Ma J, Qin QZ (2005) J Power Sources 148:66
29. Funimota K, Yasuda M, Yamashita R, Hisayuki N (1987) High Temp High Press 19:687
30. Letellier M, Chevallier F, Morcrette M (2007) Carbon 45:1025
31. Iijima T, Suzuki K, Matsuda Y (1995) Synth Met 73:9
32. Wissler M (2006) J Power Sources 156:142